JOURNAL OF THEORETICAL AND APPLIED MECHANICS
2, **40**, 2002

REGULAR AND CHAOTIC VIBRATIONS OF VAN DER POL-MATHIEU OSCILLATOR WITH NON-IDEAL ENERGY SOURCE

Jerzy Warmiński

Department of Applied Mechanics, Technical University of Lublin
email: jwar@archimedes.pol.lublin.pl

Vibrations of a parametrically and self-excited system with a non-ideal source of energy have been analysed in this paper. The model has consisted of the van der Pol-Mathieu oscillator and non-ideal energy source, which characteristic has been assumed as a straight line. Regular motion of the complete system, energy source – vibrating model, near the main parametric resonance, has been solved analytically by the applying Krilov-Bogolubov-Mitropolski method. Possible types of motion and transition from regular to chaotic motion have been investigated by using the Lyapunov's exponent criterion and attractor topological structure analysis.

Key words: non-ideal systems, chaos, parametric and self-excited vibrations, synchronisation

1. Introduction

Interaction between parametric and self-excited systems leads to many interesting phenomena. A special effect, which is called a synchronisation phenomenon, near the main and the second order parametric resonances was presented by Tondl (1978), Yano (1989). Regular vibrations of the van der Pol-Mathieu oscillator with different types of non-linearities were considered there. Parametric vibrations pulled in self-excited vibrations near parametric resonances. Outside those regions the system vibrated quasi-periodically with a modulation amplitude. Analysis of regular vibrations of a parametrically and self-excited system with the Rayleigh self-excitation model was presented by Szabelski and Warmiński (1995). The internal loop inside the main parametric

resonance, as a result of an external force influence, for one degree of freedom system was there discovered. Warmiński (2001) examined regular and chaotic vibrations of the van der Pol-Mathieu oscillator as well. It was presented there that an additional external force can cause important quantitative changes in synchronisation and chaotic regions.

The considered models were mainly assumed as ideal systems. In a certain class of models, called non-ideal, the excitation of a system can not be expressed as a pure function of time, but as an equation that relates the source of energy to the system. Hence, non-ideal systems always have one additional degree of freedom in comparison with similar ideal systems. The fundamental analysis of non-ideal system vibrations was presented by Kononenko (1969), where the dynamics of a non-ideal energy source and vibrating linear or nonlinear models was presented.

The influence of limited power supply on the stick-slip phenomena for a non-ideal self-excited vibrating model was investigated by Pontes et al. (2000). Regular vibrations of linear and nonlinear systems with self, parametric and external excitation and a non-ideal energy source were deeply investigated by Alifov and Frolov (1985). A dry friction model of self-excitation and a linear parametric excitation were considered in that paper. Two stable solutions with similar amplitudes in the resonance area were obtained for the ideal, as well for non-ideal source of energy. Regular vibrations near the main parametric resonance for the Rayleigh-Mathieu model with a non-ideal source of energy were analysed by Warmiński et al. (2001). Analytical solutions for that model were obtained by the using analytical Krilov-Bogolubov-Mitropolski method.

The aim of this paper is to analyse regular vibrations near the main parametric resonance of the van der Pol-Mathieu oscillator forced by a non-ideal energy source and to present possible transition of the system from regular to chaotic motion. The obtained results will be compared with the equivalent ideal system.

2. Model of vibrating system

Let us consider the parametric and self-excited model, which includes a direct current (DC) motor with limited power, operating on a structure. The excitation of the system is limited by the characteristic of the energy source. Vibration of the system depends on motion of the motor and the energy source motion depends on vibration of the system. Then, coupling of the vibrating

oscillator and the energy source motions takes place. Hence, it is important to analyse what happens to the motor, as the response of the system changes.

Let us take into account one degree of freedom model with a non-ideal source of energy presented in Fig. 1.

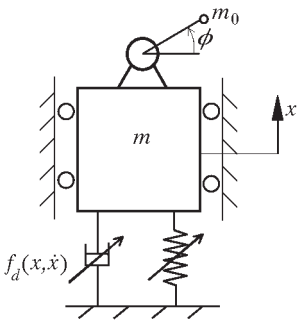

Fig. 1. Model of a non-ideal parametrically and self-excited system

The model consists of a nonlinear cubic spring with periodically changing stiffness, which represents parametric excitation of the system, and self-excitation described by the function $f_d(x, \dot{x})$. The presence of the unbalanced mass m_0 in the non-ideal model alters the potential V and kinetic T energies of the ideal and linear problem, then

$$\begin{aligned} V &= \frac{1}{2}kx^2 + m_0 g(x + r\sin\phi) \\ T &= \frac{1}{2}(I_0 + m_0 r^2)\dot{\phi}^2 + \frac{1}{2}m_0\dot{x}^2 + \dot{x}\dot{\phi}rm_0\cos\phi + \frac{1}{2}m\dot{x}^2 \end{aligned} \tag{2.1}$$

where

I_0 – moment of inertia of the rotor

r, m_0 – radius and mass of the rotating element.

Using of the second kind of Lagrange's equations, we derive differential equations of motion of the linear model

$$\begin{aligned} &(m + m_0)\ddot{x} + kx = m_0 r\dot{\phi}^2\sin\phi - m_0 r\ddot{\phi}\cos\phi \\ &(I_0 + m_0 r^2)\ddot{\phi} + H(\dot{\phi}) = L(\dot{\phi}) - m_0 r\ddot{x}\cos\phi + m_0 gr\cos\phi \end{aligned} \tag{2.2}$$

where

$H(\dot{\phi})$ – resistance torque

$L(\dot{\phi})$ – engine torque.

Taking into account that $m_0 gr\cos\phi$ is a small term and introducing nonliner terms into equations (2.2), according to the paper by Warmiński (2001), we express differential equations of motion of the complete non-ideal model in the dimensionless form

$$\ddot{X} + F_d(X,\dot{X}) + (1-\mu\cos 2\phi)(1+\gamma X^2)X = q_1(\ddot{\phi}\cos\phi - \dot{\phi}^2\sin\phi)$$
$$\ddot{\phi} = q_2\ddot{x}\cos\phi + \Gamma(\dot{\phi}) \qquad \dot{\phi} = \omega \tag{2.3}$$

where

τ – dimensionless time, $\tau = pt$

p – natural frequency of the system, $p = \sqrt{k/m_1}$

and

$$m_1 = m + m_0 \quad \dot{X} = \frac{dX}{d\tau} \qquad \ddot{X} = \frac{d^2X}{d\tau^2}$$
$$\dot{\phi} = \frac{d\phi}{d\tau} \qquad \Gamma(\dot{\phi}) = \frac{L(\dot{\phi}) - G(\dot{\phi})}{m_0 r^2 + I_0}$$
$$q_1 = \frac{m_0 r}{M + m_0} \quad q_2 = \frac{m_0 r}{I_0 + m_0 r^2}$$

The nonlinear damping function, which represents the self-excitation is assumed as a van der Pol function: $F_d(X,\dot{X}) = (-\alpha + \beta X^2)\dot{X}$, the nonlinear stiffness is expressed by the parameter γ, and the parametric excitation amplitude by μ. The parameters α, β, γ, μ, q_1, q_2 are small and positive. The system is forced by a non-ideal engine (DC motor), which characteristic is assumed as a linear function of the angular velocity (Balthazar et al., 1997)

$$\Gamma(\dot{\phi}) = u_1 - u_2\dot{\phi} \tag{2.4}$$

where

u_1 – control parameter depending on the voltage

u_2 – parameter depends on a type of the energy source.

3. Asymptotic analysis

Let us consider vibrations of the system near the main parametric resonance. Then the system vibrates with the frequency ω close to the natural frequency p ($p = 1$), while the parametric excitation frequency is 2ω.

Introducing a small parameter ε, we can write

$$p - \omega = \varepsilon\Delta \tag{3.1}$$

Let us also assume that motion of the system takes place around a steady state. It means that the second derivative $\ddot{\phi}$ is not large. Expressing the parameters by a small parameter

$$\begin{aligned} &\alpha = \varepsilon\widetilde{\alpha} && \beta = \varepsilon\widetilde{\beta} && \gamma = \varepsilon\widetilde{\gamma} \\ &\mu = \varepsilon\widetilde{\mu} && q_1 = \varepsilon\widetilde{q}_1 && q_2 = \varepsilon\widetilde{q}_2 \\ &\Gamma(\dot{\phi}) = \varepsilon\widetilde{\Gamma}(\dot{\phi}) \end{aligned}$$

the differential equations of motion take the form

$$\begin{aligned} &\ddot{X} + p^2 X = \varepsilon\Big[(\widetilde{\alpha} - \widetilde{\beta}\dot{X}^2)\dot{X} + \widetilde{\mu} X\cos 2\phi - \widetilde{\gamma}X^3 + \\ &+\widetilde{\mu}\widetilde{\gamma}X^3\cos 2\phi - \widetilde{q}_1\ddot{\phi}\cos\phi + \widetilde{q}_1\dot{\phi}^2\sin\phi \\ &\ddot{\phi} = \varepsilon\Big[\widetilde{\Gamma}(\dot{\phi}) - \widetilde{q}_2\ddot{X}\cos\phi\Big] \end{aligned} \tag{3.2}$$

Next, following Kononenko (1969), equations $(3.2)_1$ are transformed into new coordinates A, ϕ, ψ, where

$$X = A\cos(\phi+\psi) \qquad \dot{X} = -Ap\sin(\phi+\psi) \qquad \dot{\phi} = \omega \tag{3.3}$$

and the second derivative of X has the form

$$\ddot{X} = -\frac{dA}{dt}p\sin(\phi+\psi) - \Big(\omega + \frac{d\psi}{dt}\Big)Ap\cos(\phi+\psi) \tag{3.4}$$

Taking into account $(3.2)_2$ and (3.3) we obtain

$$\frac{dA}{dt}\cos(\phi+\psi) - \frac{d\psi}{dt}A\sin(\phi+\psi) = (\omega - p)A\sin(\phi+\psi) \tag{3.5}$$

Substitution of equations (3.3)-(3.5) into differential equations of motion (3.2) yields

$$\begin{aligned} \frac{d\omega}{dt} &= \varepsilon\Big[\widetilde{\Gamma}(\omega) + Ap\widetilde{q}_2\omega\cos\phi\cos(\phi+\psi)\Big] \\ \frac{dA}{dt} &= \varepsilon\Big\{-\frac{\widetilde{q}_1\omega^2}{p}\sin\phi + A\Big(\widetilde{\alpha} - \frac{1}{4}A^2\widetilde{\beta}\Big)\sin(\phi+\psi) + \frac{3}{4}\frac{A^3\widetilde{\gamma}}{p}\cos(\phi+\psi) - \\ &- \frac{A\widetilde{\mu}}{2p}\Big(1 + \frac{3}{4}A^2\widetilde{\gamma}\Big)\cos(\phi-\psi) - \frac{1}{4}A^3\widetilde{\beta}\sin 3(\phi+\psi) + \\ &+ \frac{1}{4}\frac{A^3\widetilde{\gamma}}{p}\cos 3(\phi+\psi) - \frac{A\widetilde{\mu}}{2p}\Big(1 + \frac{3}{4}A^2\widetilde{\gamma}\Big)\cos(3\phi+\psi) - \end{aligned} \tag{3.6}$$

$$- \quad \frac{1}{8}\frac{A^3\widetilde{\gamma}\widetilde{\mu}}{p}\cos(\phi+3\psi) - \frac{1}{8}\frac{A^3\widetilde{\gamma}\widetilde{\mu}}{p}\cos(5\phi+3\psi)\Big\}\sin(\phi+\psi) + \varepsilon^2...$$

$$\frac{d\psi}{dt} = \varepsilon\Big\{\Delta - \frac{\widetilde{q}_1\omega^2}{Ap}\sin\phi + \Big(\widetilde{\alpha} - \frac{1}{4}A^2\widetilde{\beta}\Big)\sin(\phi+\psi) - \frac{1}{4}A^2\widetilde{\beta}\sin 3(\phi+\psi) +$$
$$+ \quad \frac{3}{4}\frac{A^2\widetilde{\gamma}}{p}\cos(\phi+\psi) + \frac{1}{4}\frac{A^2\widetilde{\gamma}}{p}\cos 3(\phi+\psi) - \frac{1}{2}\frac{\widetilde{\mu}}{p}\cos(\phi-\psi) -$$
$$- \quad \frac{1}{2}\frac{\widetilde{\mu}}{p}\cos(3\phi+\psi) - \frac{1}{8}\frac{A^2\widetilde{\gamma}\widetilde{\mu}}{p}\cos(5\phi+3\psi)\Big\}\cos(\phi+\psi) + \varepsilon^2...$$

To solve equations (3.6) the classical Krilov-Bogolubov-Mitropolski method is applied. According to this method, in the first approximation we can write

$$\begin{aligned} \omega &= \Omega + \varepsilon U_1(\phi, \Omega, a, \xi) \\ A &= a + \varepsilon U_2(\phi, \Omega, a, \xi) \\ \psi &= \xi + \varepsilon U_3(\phi, \Omega, a, \xi) \end{aligned} \tag{3.7}$$

where $U_i(\phi, \Omega, a, \xi)$, $i = 1, 2, 3$ are slowly changing periodic functions of time. To find solutions for Ω, a, ξ in the first approximation the right sides of equations (3.6) are averaged

$$\frac{d\Omega}{dt} = \frac{\varepsilon}{2\pi}\int_0^{2\pi} f_\Omega\, d\varphi \qquad \frac{da}{dt} = \frac{\varepsilon}{2\pi}\int_0^{2\pi} f_a\, d\varphi \qquad \frac{d\xi}{dt} = \frac{\varepsilon}{2\pi}\int_0^{2\pi} f_\xi\, d\varphi \tag{3.8}$$

and after integration we obtain

$$\begin{aligned} \frac{d\Omega}{dt} &= \varepsilon\Big[\widetilde{\Gamma}(\Omega) - \frac{1}{2}ap\widetilde{q}_2\Omega\cos\xi\Big] \\ \frac{da}{dt} &= \varepsilon\Big[\frac{1}{2}\widetilde{\alpha}a - \frac{1}{8}a^3\widetilde{\beta} - \frac{1}{4}a\frac{\widetilde{\mu}}{p}\sin 2\xi - \frac{1}{8}a^3\frac{\widetilde{\gamma}\widetilde{\mu}}{p}\sin 2\xi - \frac{1}{2}\widetilde{q}_1\frac{\Omega^2}{p}\cos\xi\Big] \\ \frac{d\xi}{dt} &= \varepsilon\Big[\Delta + \frac{3}{8}a^2\frac{\widetilde{\gamma}}{p} - \frac{1}{4}\frac{\widetilde{\mu}}{p}\cos 2\xi - \frac{1}{4}\frac{\widetilde{\gamma}\widetilde{\mu}}{p}\cos 2\xi + \frac{1}{2}\widetilde{q}_1\frac{\Omega^2}{ap}\sin\xi\Big] \\ \frac{d\phi}{dt} &= \Omega \end{aligned} \tag{3.9}$$

For the steady state, equations (3.9) have the form

$$\widetilde{\Gamma}(\Omega) - \frac{1}{2}ap\widetilde{q}_2\Omega\cos\xi = 0$$

$$\frac{1}{2}\widetilde{\alpha}a - \frac{1}{8}a^3\widetilde{\beta} - \frac{1}{4}a\frac{\widetilde{\mu}}{p}\sin 2\xi - \frac{1}{8}a^3\frac{\widetilde{\gamma}\widetilde{\mu}}{p}\sin 2\xi - \frac{1}{2}\widetilde{q}_1\frac{\Omega^2}{p}\cos\xi = 0 \tag{3.10}$$
$$\Delta + \frac{3}{8}a^2\frac{\widetilde{\gamma}}{p} - \frac{1}{4}\frac{\widetilde{\mu}}{p}\cos 2\xi - \frac{1}{4}\frac{\widetilde{\gamma}\widetilde{\mu}}{p}\cos 2\xi - \frac{1}{2}\widetilde{q}\frac{\Omega^2}{ap}\sin\xi = 0$$

and then the angular velocity, amplitude and phase of the vibrating system for the steady state can be obtained from the above equations.

4. Stability analysis

The stability analysis of the periodic solutions is performed by using approximate differential equations of the first order (3.9), which can be written in a shortened form

$$\frac{d\Omega}{dt} = F_1(a,\Omega,\xi) \qquad \frac{da}{dt} = F_2(a,\Omega,\xi) \qquad \frac{d\xi}{dt} = F_3(a,\Omega,\xi) \tag{4.1}$$

In the steady state, equations (4.1) are equal to zero

$$F_1(a,\Omega,\xi) = 0 \qquad F_2(a,\Omega,\xi) = 0 \qquad F_3(a,\Omega,\xi) = 0$$

Taking into account a difference between perturbed and not perturbed equations, the differential equations in variations are written as follows

$$\begin{aligned}
\frac{d\delta_\Omega}{dt} &= \Big(\frac{\partial F_1}{\partial\Omega}\Big)_0\delta_\Omega + \Big(\frac{\partial F_1}{\partial a}\Big)_0\delta_a + \Big(\frac{\partial F_1}{\partial\xi}\Big)\delta_\xi \\
\frac{d\delta_a}{dt} &= \Big(\frac{\partial F_2}{\partial\Omega}\Big)_0\delta_\Omega + \Big(\frac{\partial F_2}{\partial a}\Big)_0\delta_a + \Big(\frac{\partial F_2}{\partial\xi}\Big)\delta_\xi \\
\frac{d\delta_\xi}{dt} &= \Big(\frac{\partial F_3}{\partial\Omega}\Big)_0\delta_\Omega + \Big(\frac{\partial F_3}{\partial a}\Big)_0\delta_a + \Big(\frac{\partial F_3}{\partial\xi}\Big)\delta_\xi
\end{aligned} \tag{4.2}$$

Characteristic determinant of equation (4.2) has the form

$$\begin{vmatrix}
\Big(\frac{\partial F_1}{\partial\Omega}\Big)_0\delta_\Omega - \rho & \Big(\frac{\partial F_1}{\partial a}\Big)_0\delta_a & \Big(\frac{\partial F_1}{\partial\xi}\Big)\delta_\xi \\
\Big(\frac{\partial F_2}{\partial\Omega}\Big)_0\delta_\Omega & \Big(\frac{\partial F_2}{\partial a}\Big)_0\delta_a - \rho & \Big(\frac{\partial F_2}{\partial\xi}\Big)\delta_\xi \\
\Big(\frac{\partial F_3}{\partial\Omega}\Big)_0\delta_\Omega & \Big(\frac{\partial F_3}{\partial a}\Big)_0\delta_a & \Big(\frac{\partial F_3}{\partial\xi}\Big)\delta_\xi - \rho
\end{vmatrix} = 0 \tag{4.3}$$

Index "0" denotes partial derivatives of F functions in the equilibrium point. Stability of approximate solutions (3.9) depends on the roots of characteristic equation (4.3). The solutions are stable if the eigenvalues of the characteristic equation have negative real parts.

5. Regular vibrations

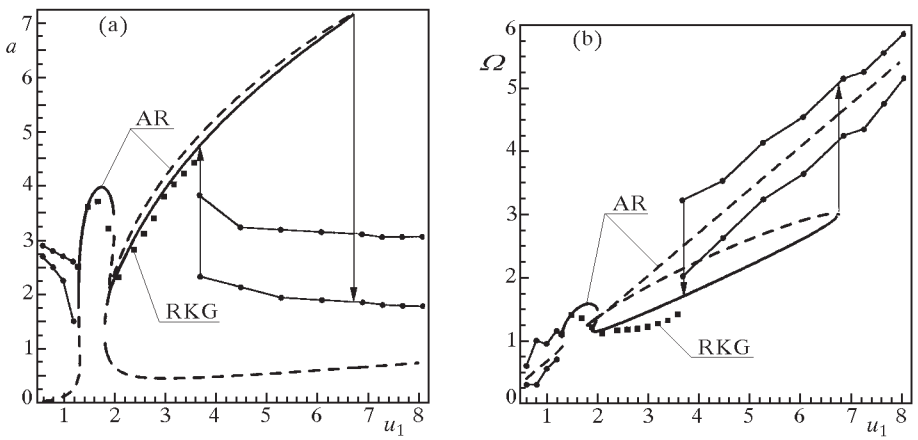

Fig. 2. Vibrations near the main parametric resonance versus control parameter u_1, (a) amplitude, (b) angular velocity

Numerical results were carried out by using Matlab-Simulink® package. The calculations were done for the system parameters taken from the most interesting intervals of physical systems, see Warmiński (2001) and Balthazar et al. (1997). Values of parameters are following

$$\begin{aligned} &\alpha = 0.1 \quad \beta = 0.05 \quad \gamma = 0.1 \\ &\mu = 0.2 \quad q_1 = 0.2 \quad q_2 = 0.3 \end{aligned} \tag{5.1}$$

and the characteristic of the energy source was assumed as a straight line (3.4). In our calculations the control parameter is assumed as $u_1 \in (0.5, 8.0)$ and $u_2 = 1.5$. Taking into account approximate equations (3.10) and finding numerically the roots of characteristic equation (4.3) we plotted the amplitude and angular velocity versus the control parameter (Fig. 2). Stable and unstable analytical solutions (AR) are marked by solid and dashed lines respectively,

small squares denotes numerical results obtained by Runge-Kutta-Gill method (RKG) with a variable integration step length. Increasing the control parameter u_1 in interval $u_1 \in (0.5, 1.3)$, we observe quasi-periodic motion, which is obtained by mutual interaction between the self-excitation, parametric excitation and energy source (DC motor). This type of motion is shown in Fig. 2 by two dots, corresponding to the extreme deflections of the system. In the region $u_1 \in (1.3, 6.75)$, kind of a synchronisation effect is observed. It is predominated by the parametric and external excitation. An interesting effect in the synchronisation region is visible. There are two maxima, resulting from strong interaction between the vibrating system and energy source (limited power supply). At the beginning, the amplitude increases, then decreases and jumps to the second part of the stable resonance curve and increases once again. Going out from the synchronisation area, the system jumps from periodic to quasi-periodic motion and finally vibrates quasi-periodically. When the parameter u_1 is decreasing, the jump phenomenon from the quasi-periodic to periodic motion takes place around $u_1 =\sim 3.75$. It means that in the interval $u_1 \in (3.75, 6.75)$, the periodic and quasi-periodic motion can appear, depending on initial conditions.

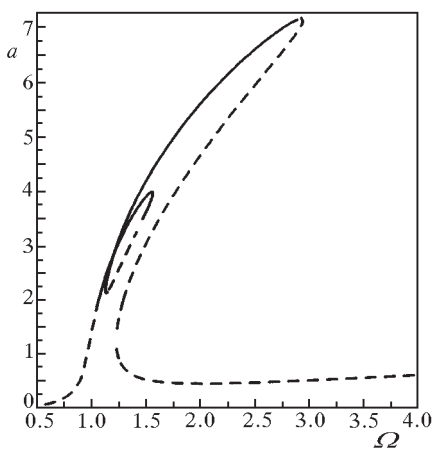

Fig. 3. Amplitude versus angular velocity near the main parametric resonance

Similar effects connected with the angular velocity are shown in Fig. 2b. It is necessary to underline that, inside the synchronisation region, we also observe a local minimum of the angular velocity Ω. The amplitude characteristic versus angular velocity near the main parametric resonance obtained from asymptotic analysis is presented in Fig. 3. This resonance curve has not a

typical shape. Inside the synchronisation region a internal loop appears. It can be explained while observing the synchronisation region in Fig. 2a and Fig. 2b. Comparing the amplitude and angular velocity characteristics, the local maximum for both curves is visible. It affects directly the shape of the amplitude versus angular velocity curve (Fig. 3). The appearing internal loop was also observed for the ideal model (Warmiński, 2001). Nevertheless, ideal and non-ideal loops have different features. For the ideal model the internal loop appears on the right branch of the resonance curve and only its upper part is stable. For the non-ideal van der Pol oscillator the loop appears on the left branch and there are stable solutions, however a piece of the lower part is unstable. This effect is caused by the interaction between the self and parametric excitations and due to the influence of the non-ideal source of energy. This is a different result than that obtained for the non-ideal Rayleigh oscillator where the loop was completely stable, see Warmiński et al. (2001).

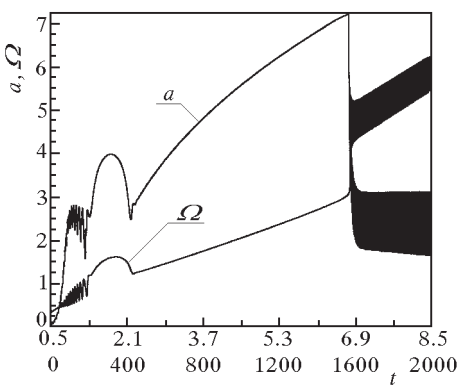

Fig. 4. Transition through resonance with a slowly increasing value of the control parameter u_1

Additionally, approximate equations of motion (3.9) were modelled in the Matlab-Simulink package and were solved by the RKG method. The control parameter was slowly increased in time (Fig. 4). The time axis has two scales: the time scale and corresponding u_1 scale. The simulation of the averaged equations shows evidently quasi-periodic motion out of the resonance region and periodic (synchronised) motion inside the main parametric resonance. Local decreasing of the amplitude and angular velocity is also visible. Behaviour of the system for decreasing parameter u_1 presents Fig. 5. Coming into the synchronisation area takes place near $t = 1250$ ($u_1 = 3.75$). The dynamic hysteresis effect is then visible.

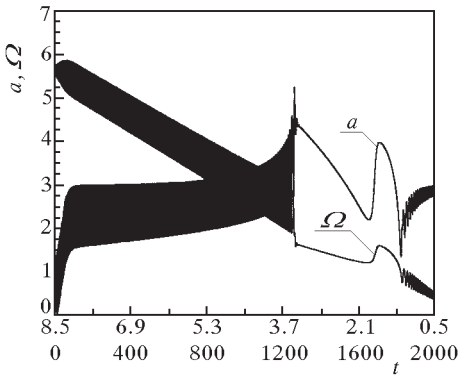

Fig. 5. Transition through resonance with a slowly increasing value of the control parameter u_1

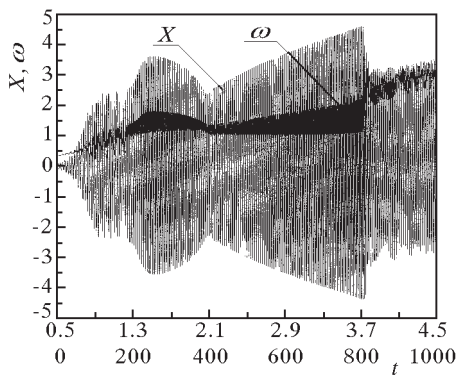

Fig. 6. Transition through resonance with a slowly increasing value of the control parameter u_1, numerical simulation

To confirm the analytical investigation, equations (3.2) were directly solved numerically. Fig. 6 and Fig. 7 present numerical results obtained for the passage through resonance with slowly increasing and decreasing value of the control parameter u_1. In these figures one can notice that inside the resonance region, $t \in (200, 820)$ – for increasing and $t \in (280, 850)$ – for decreasing values of the control parameter u_1, two maxima of the amplitude are visible. These results are in agreement with the previous analytical results shown in Fig. 2 and Fig. 4. The difference is in the synchronisation width. The synchronisation area obtained from the direct simulation is smaller than that obtained from the analytical approach. Nevertheless, the main behaviour is the same.

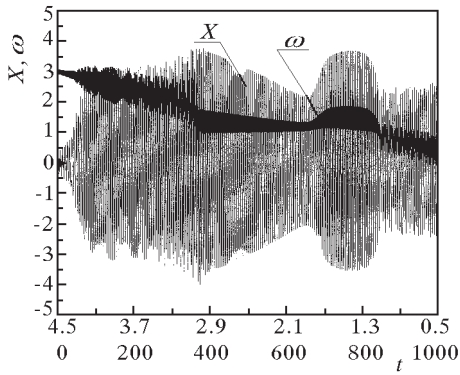

Fig. 7. Transition through resonance with a slowly decreasing value of the control parameter u_1, numerical simulation

6. Chaotic vibrations

The system of differential equations (2.3) was solved numerically by using the Runge-Kutta forth order method and numerical results were carried out by the Dynamics package (Nusse and York, 1994). All simulations were done on the DecAlpha 200 workstation. To classify different types of motion, the maximal Lyapunov exponent criterion was applied. At the beginning the Lyapunov exponent diagram versus control parameter u_1 was calculated for assumed parameters (5.1). Results are presented in Fig. 8.

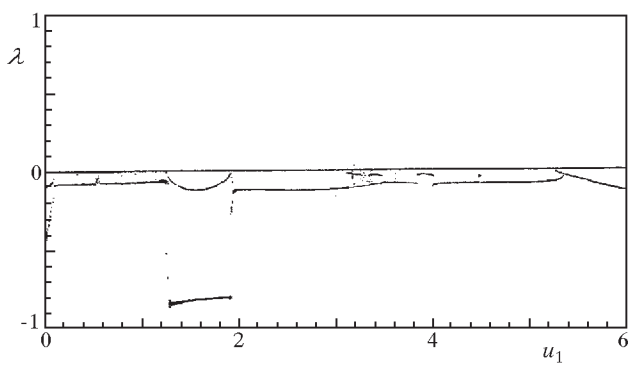

Fig. 8. Lyapunov exponents diagram versus control parameter u_1

In the whole considered region $u_1 \in (0, 6)$, the maximal Lyapunov exponent is not greater than zero (has not positive sign). It means that the system vibrates regularly. Phase diagrams (Fig. 9) demonstrates possible different types of regular motion.

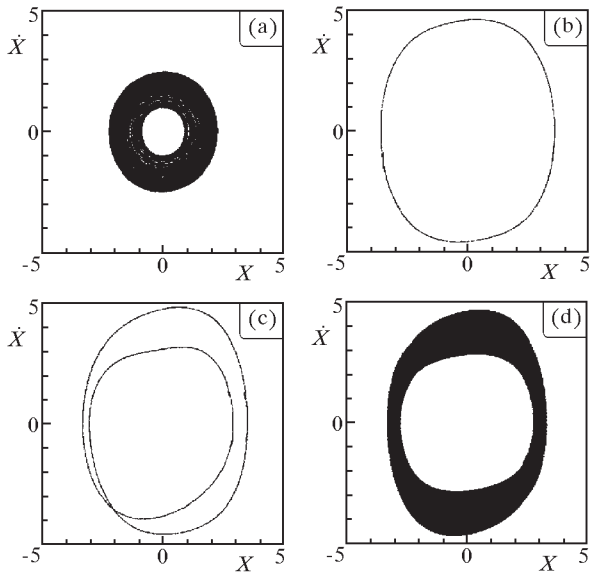

Fig. 9. Phase diagrams for chosen parameters u_1, (a) $u_1 = 1.25$, (b) $u_1 = 1.5$, (c) $u_1 = 3.2$, (d) $u_1 = 3.5$

The phase diagram in Fig. 9a presents vibration of the non-ideal system before the main parametric resonance. The obtained attractor represented by a black area ("torus") on the phase plane corresponds to quasi-periodic motion of the system, out of the synchronisation region. For larger value of u_1 parameter, the parametric excitation frequency synchronises with the self-excitation and with rotation of the motor. Then a synchronisation phenomenon takes place. In the phase diagram (Fig. 9b) periodic motion is observed. This kind of vibration corresponds to the region $u_1 \in (\sim 1.3, \sim 1.95)$ in Fig. 8. Having gone out from this region the system vibrates quasi-periodically once again. The second synchronisation effect occurs in a smaller interval around $u_1 \in (\sim 3.15, \sim 3.45)$. Nevertheless, in that case of synchronisation, periodic motion has two times larger period than that in the previous case. For $u_1 = 3.5$ the system is out of the second synchronisation region and vibrates quasi-periodically (Fig. 9d). Values of the Lyapunov exponents for the considered phase diagrams are presented in Table 1.

Table 1. Lyapunov exponents for chosen u_1 parameters

u_1	attractor type	λ_1	λ_2	λ_3	λ_4
1.25	quasi-periodic	0	0	−0.062	−1.465
1.5	periodic	0	−0.118	−0.824	−0.824
3.2	periodic	0	−0.027	−0.027	−1.640
3.5	quasi-periodic	0	0	−0.084	−1.588

Periodic motion of the system takes place if the maximal value of the Lyapunov exponent is equal to zero. For quasi-periodic motion two Lyapunov exponents are equal to zero. This analysis shows that the system motion is evidently regular.

Basing on the results obtained for the ideal system (Warmiński, 2001), we can mention that the increase of the parametric excitation amplitude μ leads to chaos. The transition from regular to chaotic motion of the ideal system was possible for $\mu > 1$.

Let us assume that in the considered non-ideal model, the parametric excitation slightly increases to value $\mu = 0.4$ and the rest of parameters save their values. A diagram with Lyapunov exponents for this case is plotted in Fig. 10.

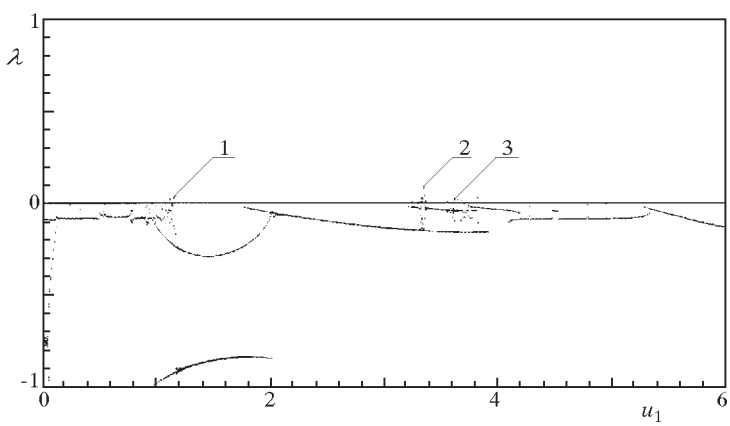

Fig. 10. Lyapunov exponents versus control parameter u_1, $\mu = 0.4$

In Fig. 10 we can recognise three regions where the maximal Lyapunov exponent has small but positive value (marked by no. 1, 2, 3). It means, that in these three intervals of u_1 parameter, the system vibrates chaotically. The next diagram (Fig. 11), plotted for $\mu = 1.0$, shows that those chaotic regions increase significantly. The maximal Lyapunov exponent achieves much greater positive values and chaotic areas are wider. The first chaotic region

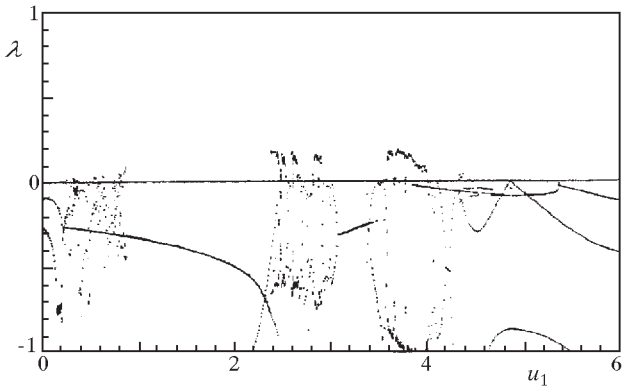

Fig. 11. Lyapunov exponents diagram control parameter u_1, $\mu = 1.0$

appears before the synchronisation, for small values of the control parameter $u_1 \in (0.6, 0.95)$. Two additional chaotic regions occur for $u_1 \in (2.4, 2.7)$ and $u_1 \in (3.6, 4.0)$. The Lyapunov exponent in the second and third regions achieve considerable bigger values than in the first one.

Each of the chaotic regions possesses small windows of regular motion. Transition from regular to chaotic motion is presented in Poincare's maps (Fig. 12). The regular attractor visible in Fig. 12a obtained for $u_1 = 0.8$, transforms itself into a strange chaotic attractor with a characteristic fractal structure for $u_1 = 0.82$. In the first chaotic region regular motion can also appear (Fig. 12c). In Fig. 12d a synchronisation effect takes place, only periodic motion occurs there, mapped by a simple single attractor. From this region, the system tends to the second chaotic region (Fig. 12e). For $u_1 = 2.8$ the fractal structure gradually disappears (Fig. 12f) and vibrations go to regular form (Fig. 12g). The strange chaotic attractor in the third region presents Fig. 12h. After exceeding the limit value $u_1 = 4.0$ the system makes an exit from chaos to regular motion. Values of the Lyapunov exponents for the analysed Poincare's maps are presented in Table 2.

For the parameters $u_1 = 0.82$, $u_1 = 2.6$, $u_1 = 2.8$, $u_1 = 3.6$ the maximal Lyapunov exponent is positive. It confirms the results visible on Poincare's sections where the strange chaotic attractors with a fractal structure are plotted.

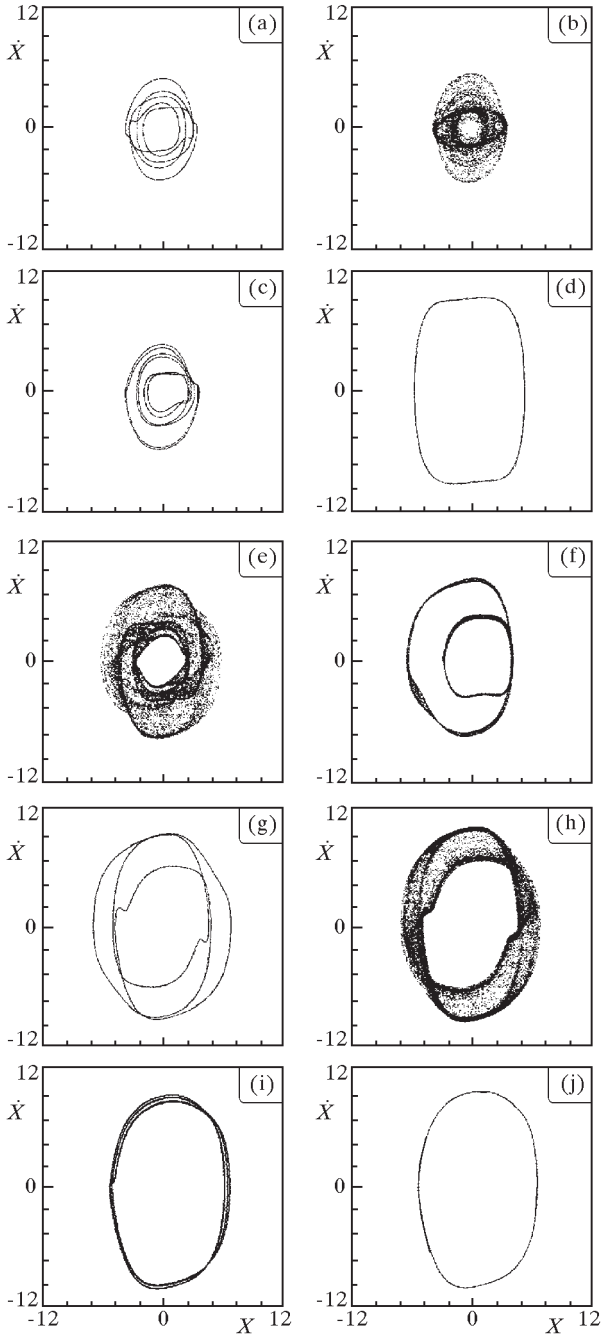

Fig. 12. Poincare's maps for different u_1 parameter (a) $u_1 = 0.8$, (b) $u_1 = 0.82$, (c) $u_1 = 0.84$, (d) $u_1 = 2.2$, (e) $u_1 = 2.6$, (f) $u_1 = 2.8$, (g) $u_1 = 3.5$, (h) $u_1 = 3.6$, (i) $u_1 = 4.0$, (j) $u_1 = 4.2$

Table 2. Lyapunov exponents for chosen u_1 parameters, $\mu = 1.0$

u_1	attractor's type	λ_1	λ_2	λ_3	λ_4
0.8	periodic	0.0	−0.055	−0.442	−1.184
0.82	chaotic	0.04	0.0	−0.265	−1.425
0.84	periodic	0.0	−0.0025	−0.201	−1.472
2.2	periodic	0.0	−0.5823	−0.5823	−0.9533
2.6	chaotic	0.16	0.0	−0.657	−1.3632
2.8	chaotic	0.026	0.0	−0.603	−1.37
3.5	periodic	0.0	−0.211	−0.884	−1.347
3.6	chaotic	0.17	0.0	−0.882	−1.593
4.0	periodic	0.0	−0.012	−0.923	−1.419
4.2	periodic	0.0	−0.508	−0.508	−1.397

7. Conclusions and remarks

This paper completes an analysis of parametric and self-excited systems taking into consideration regular and chaotic motions of a non-ideal system. Applying the analytical Krilov-Bogolubov-Mitropolski method, it is presented that near the main parametric resonance kind of a synchronisation effect takes place. Nevertheless, transition through the resonance region has different features to the equivalent ideal system. In the synchronisation region, there appear two maxima and one local minimum as well for the amplitude of the vibrating system, as for the angular velocity of the motor. This effect causes that the amplitude curve versus excitation frequency has an additional internal loop. The loop appears on the left branch of the curve and its lower part is partially unstable. Outside the synchronisation region the system vibrates quasi-periodically. This result is quite different in comparison with that obtained for the ideal van der Pol-Mathieu oscillator where the loop appeared on the right branch and its lower part was completely unstable. For a small value of the parametric excitation the system can vibrate regularly. Then, it is possible to get two types of regular motions: periodic and quasi-periodic. If the parametric excitation increases, the response of the system complicates. A small increase in the parametric excitation value, from $\mu = 0.2$ to $\mu = 0.4$, causes occurrence of three chaotic regions. Further increase of the parametric excitation leads to widening of the chaotic region, larger positive values of the Lyapunov exponents and, consequently, to more complicated behaviour

of the system. Transitions from the quasi-periodic motion to synchronisation areas and from regular to chaotic vibrations were presented by observing the attractors topology in the phase plane and Poincare's section as well as by the Lyapunov exponent criterion. For the ideal system transition to chaos was possible only for big values of the parametric excitation ($\mu > 1$). The considered non-ideal system demonstrates transition from regular to chaotic motion for smaller values of the parametric excitation $\mu = 0.4$.

References

1. Alifov A.A., Frolov K.W., 1985, *Interaction of Nonlinear Oscillatory Systems with Energy Sources* (in Russian), Nauka, Moscow
2. Balthazar J.M., Rente M.L., Davi V.M., et al., 1997, Some observations on numerical simulations of a nonlinear non-ideal problem, nonlinear dynamics, in *Chaos, Control, and Their Applications To Engineering Sciences*, Edit. Balthazar J.M., Mook D.T., Rosario J.M., Vol 1, American Academy of Mechanics and Associacao Brasileira de Ciencias Mecanicas, Brazil, ISBN 85-900351-1-5, 97-104
3. Kononenko V.O., 1969, *Vibrating Systems with Limited Power Supply*, Illife
4. Nusse H.E., Yorke J.A., 1994, *Dynamics: Numerical Explorations*, Springer Verlag, New York
5. Pontes B.R., Oliveira V.A., Balthazar J.M., 2000, On friction-driven vibrations in a mass block-belt-motor driven with a limited power supply, *Journal of Sound and Vibration*, **234**, 4, 713-723
6. Szabelski K., Warmiński J., 1995a, Self-excited system vibration with parametric and external excitations, *Journal of Sound and Vibration*, **187**, 4, 595-607
7. Szabelski K., Warmiński J., 1995b, The parametric self excited non-linear system vibrations analysis with the inertial excitation, *Journal of Non-Linear Mechanics*, **30**, 2, 179-189
8. Tondl A., 1978, On the interaction between self-excited and parametric vibrations, *Monographs and Memoranda*, **25**, National Research Institute for Machine Design, Prague
9. Warmiński J., 2001, Synchronisation effects and chaos in van der Pol-Mathieu oscillator, *Journal of Theoretical and Applied Mechanics*, **39**, 4, 861-884
10. Warmiński J., Balthazar J.M., Brasil R.M.L.R.F., 2001, Vibrations of non-ideal parametrically and self-excited model, *Journal of Sound and Vibration*, **245**, 2, 363-374

11. Yano S., 1989, Considerations on self-and parametrically excited vibrational systems, *Ingenieur-Archiv*, **59**, 285-295

Drgania regularne i chaotyczne oscylatora van der Pola-Mathieu z nieidealnym źródłem energii

Streszczenie

W pracy przeprowadzono analizę drgań układu parametryczno-samowzbudnego z nieidealnym źródłem energii. Model składa się z oscylatora van der Pola-Mathieu oraz nieidealnego źródła energii, którego charakterystykę założono w postaci linii prostej. Drgania regularne całego systemu, źródło drgań – model drgający, zostały określone w otoczeniu głównego rezonansu parametrycznego na drodze badań analitycznych z zastosowaniem metody Krilova-Bogolubova-Mitropolskiego. Możliwe typy ruchów oraz przejście układu do ruchu chaotycznego prześledzono poprzez zastosowanie kryterium wykładnika Lapunowa oraz analizę struktury topologicznej atraktorów.

Manuscript received January 8, 2001; accepted for print November 14, 2001